

Supporting Information

Tunable Quantum Dot Arrays as Efficient Sensitizers for Enhanced Near-infrared Electroluminescence of Erbium ions

Xiaowei Zhang, Tao Lin, Pei Zhang, Hucheng Song, Han Jin, Jian Xu, Jun Xu, Pengjun Wang*, Kaiyang Niu, and Kunji Chen.*

Dr. X. Zhang, Dr. P. Zhang, Dr. H. Song, Prof. J. Xu, Prof. K. Chen
National Laboratory of Solid State Microstructures
Collaborative Innovation Center of Advanced Microstructures
Department of Electronic Science and Engineering,
Nanjing University, Nanjing, 210093, China
E-mail: junxu@nju.edu.cn

Dr. X. Zhang, Prof. H. Jin, Prof. J. Xu, Prof. P. Wang
Department of Electrical Engineering and Computer Science,
Ningbo University, Ningbo, 315211, China
E-mail: wangpengjun@nbu.edu.cn

Prof. T. Lin
Laboratory of Optoelectronic Materials and Detection Technology,
Guangxi Key Laboratory for Relativistic Astrophysics,
Department of Physical Science and Technology,
Guangxi University, Nanning, 530004, China

Dr. K. Niu
Materials Sciences Division,
Lawrence Berkeley National Laboratory, Berkeley, CA, 94720, United States

Table of Contents

Figure S1. Typical cross-sectional high-resolution TEM images of SnO ₂ QDs doped silica matrix prepared with increasing metallic cations doping amounts from 5 mol% to 20 mol% in precursor.....	3
Table S1. Relationships between band gaps and average sizes of SnO ₂ QDs after annealing at different temperatures.....	4
Figure S2. (a) XRD pattern of the SnO ₂ QDs doped SiO ₂ samples after annealing 1000°C. (b) Comparison of XRD spectra of pure and Er ³⁺ ions doped SnO ₂ QDs samples.....	5
Figure S3. Near-infrared EL emission spectra of Er ³⁺ ions sensitized by SnO ₂ QD arrays with different average sizes. The forward voltage is kept at 7.5V.....	6
Figure S4. Visible EL emission spectra at the turn-on voltage at room temperature.....	6
Figure S5. (a). Characteristics of current density-voltage (<i>J-E</i>) of the devices under the forward bias condition. (b) and (c). Fowler-Nordheim (F-N) tunneling plots based on the $\ln(J/E^2)-E^{-1}$ relation and Poole-Frenkel (P-F) thermionic tunneling plots according to the $\ln(J/E)-E^{1/2}$ relation are investigated respectively for all samples.....	7
Figure S6. Flat-band energy level diagram of EL device.....	9

1. Preparation of QD arrays with controllable average size and number density

Cross-sectional TEM results characterization indicates the fact that the average size and number density can be effectively controlled by adjustments of metallic cations doping amounts in precursor and post-annealing temperature. According to our previous work by use of similar synthesis process, the average diameter of ZnO QDs^[1], In₂O₃ QDs^[2], and SnO₂ QDs^[3,4] can be controlled from ~2.0 nm to 11.0 nm with increasing annealing temperature from 400°C to 1000°C, respectively. **Figure S1** displays that the number density of crystalline SnO₂ clusters inside the silica film increases from $3.0 \times 10^{17} \text{cm}^{-3}$ to $4.4 \times 10^{18} \text{cm}^{-3}$ with increasing doping amounts of metallic cations in precursor.

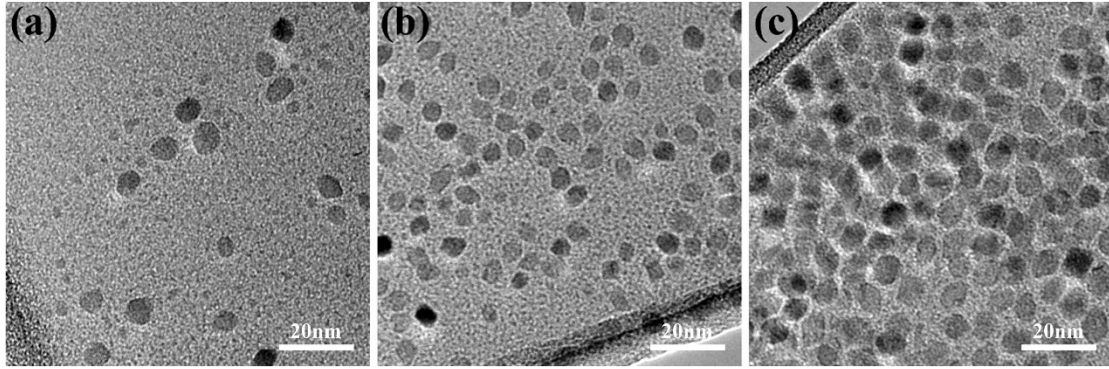


Figure S1. Typical cross-sectional high-resolution TEM images of SnO₂ QDs doped silica matrix prepared with increasing metallic cations doping amounts from 5 mol% to 20 mol% in precursor.

2. Redshift of excitation band corresponding to Effective Mass Theory.

The redshifts of the excitation from band-to-band transition of SnO₂ QDs can be explained as the enlargement of the average sizes with increasing annealing temperatures. Based on these excitation peaks, we also estimated the average size of SnO₂ QDs by use of the Effective Mass Theory,^[5]

$$E_g(R) = E_g(R \rightarrow \infty) + \frac{h^2}{8R^2} \times \left(\frac{1}{m_e^*} + \frac{1}{m_h^*} \right) - \frac{1.8e^2}{4\pi\epsilon_r\epsilon_0 R} + \text{smaller terms},$$

where $E_g(R)$ is the band gap energy of SnO₂ QDs, R is the average radius of SnO₂

QDs, $E_g(R \rightarrow \infty)$ is the band gap energy of SnO₂ bulk materials and ε_r is the relative dielectric constant. m_e^* and m_h^* stand for the effective mass of an electron and a hole, respectively. For SnO₂ QDs,

$$E_g(R \rightarrow \infty) = 3.6 \text{ eV},$$

$$\varepsilon_r = 14,$$

$$\varepsilon_0 = 8.85 \times 10^{-12} \text{ F/m},$$

$$m_e^* = 0.35m_0, m_h^* = m_e^*,$$

where m_0 stands for the free electron mass. Meanwhile, $E_g(R)$ can be calculated as follows,

$$E_g(R) = \frac{1240}{\lambda_{exc}},$$

where λ_{exc} stands for the excitation peak from band-to-band transition of SnO₂ QDs. As shown in **Table S1**, it is found that the average sizes of SnO₂ QDs with different annealing temperatures are consistent with previous TEM observations.

Table S1. Relationships between band gaps and average sizes of SnO₂ QDs after annealing at different temperatures.

Annealing temperature / °C	800	900	1000	Bulk materials
λ_{exc} / nm	293	300	322	~344
Band gap / eV	4.23	4.13	3.85	3.60
Average size / nm	2.92	4.22	5.12	—

3. Comparison of XRD spectra of pure and Er³⁺ ions doped SnO₂ QDs samples

Generally, the Er³⁺ ions are very hard to dissolve in Sn⁴⁺ sites due to the large radius mismatch and the charge imbalance (0.088nm for Er³⁺ ions, 0.071 nm for Sn⁴⁺ ions).

However, it has been reported recently that the Er^{3+} ions were successfully doped into SnO_2 QDs with Er^{3+} ions doping concentration of 0.043 at.% according to the experimental results using an Ultima2 ICP-OES (inductively coupled plasma optical emission spectrometer).^[6] On the other hand, according to the quantitative studies of PL decay lifetime and photoluminescence temperature-dependence, our previous work^[7] also indicated that parts of Er^{3+} ions remain in the amorphous silica matrix and the others may be trapped in the SnO_2 QDs, similar to that of Eu^{3+} in SnO_2 QDs reported before^[8]. EDS elemental mapping reveals the fact that a small fraction of Er^{3+} ions get incorporated at the interstitial sites though most of them could be segregated to the surface of the SnO_2 QDs. In order to further confirm the location of Er^{3+} ions, we also perform X-ray diffraction measurement as shown in Figure S3. The related XRD spectra express a slight shifting, revealing the fact that Er^{3+} ions may be very likely incorporated in the D_{2h} lattice site of Sn^{4+} . Though the present results need to further investigation, we believe that the partial incorporation of Er^{3+} ions into the SnO_2 sites plays a significant role in the enhancement of sensitization efficiency.

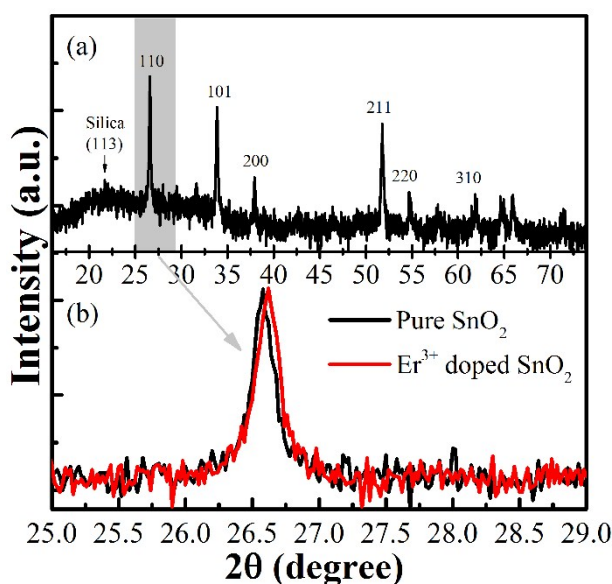


Figure S2. (a) XRD pattern of SnO_2 QDs doped SiO_2 samples after annealing 1000°C . (b) Comparison of XRD spectra of pure and Er^{3+} ions doped SnO_2 QDs samples.

4. Near-infrared electroluminescence of Er^{3+} ions sensitized by SnO_2 QD arrays with

different average sizes.

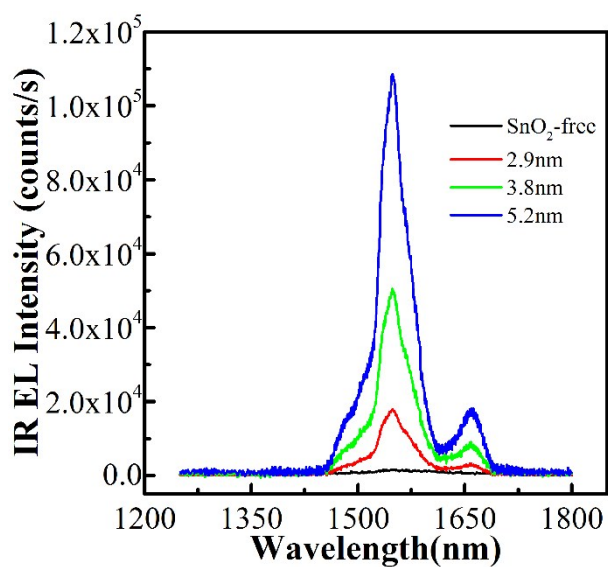


Figure S3. Near-infrared EL emission spectra of Er³⁺ ions sensitized by SnO₂ QD arrays with different average sizes. The forward voltage is kept at 7.5V.

5. Visible EL emission at the turn-on voltage

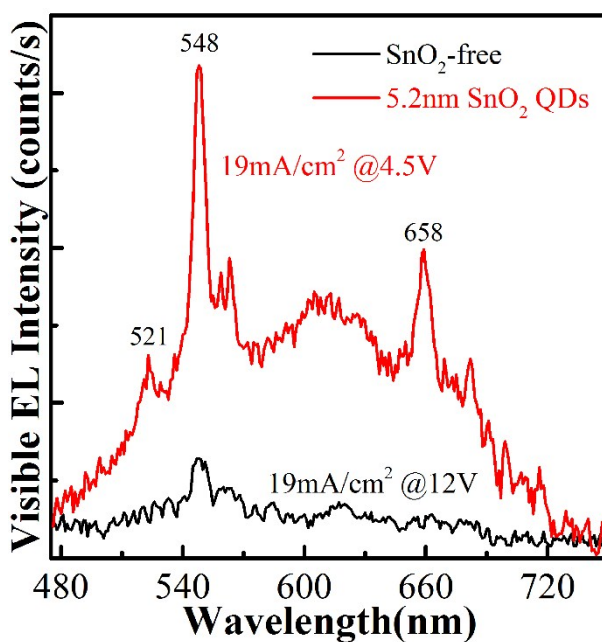


Figure S4. Visible EL emission spectra of Er³⁺ ions at the turn-on voltage.

6. Descriptions of the carriers' transport mechanism

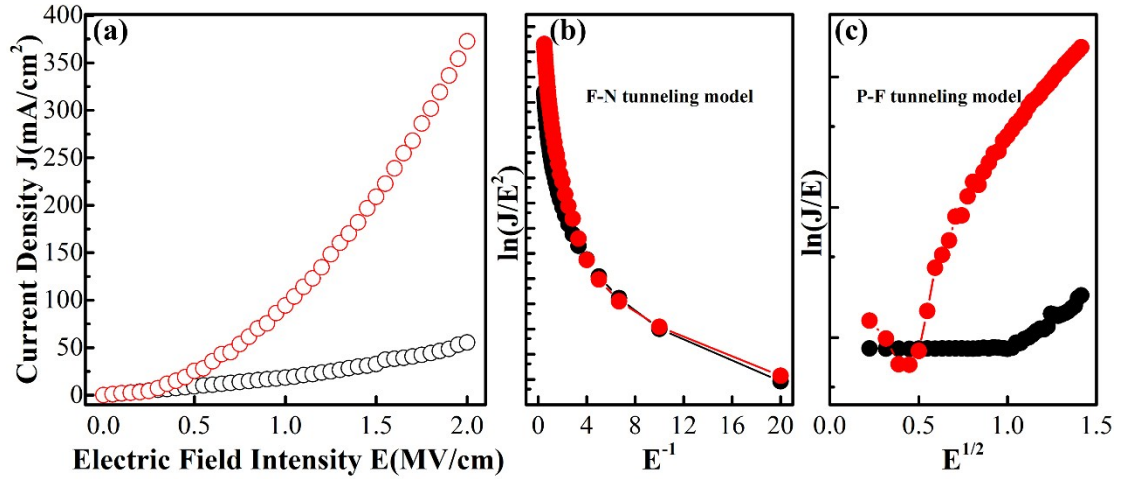


Figure S5. (a). Characteristics of current density-voltage (J - E) of the devices under the forward bias condition. (b) and (c). Fowler-Nordheim (F-N) tunneling plots based on the $\ln(J/E^2)$ - E^{-1} relation and Poole-Frenkel (P-F) thermionic tunneling plots according to the $\ln(J/E)$ - $E^{1/2}$ relation are investigated respectively for all samples. E is in MV/cm.

7. The estimations of detailed estimations of acceleration length and kinetic energy of hot electrons for pure amorphous silica matrix.

The acceleration length and kinetic energy of hot electrons can be calculated as follows. As shown in Figure 5e, for the SnO₂-free sample, the electrical transport of carriers can be well explained by the power law of the space charge limited current (SCLC) mechanism. Due to the non-crystalline nature of silica matrix, the injected carriers from both top and bottom electrodes are instantly localized by the trap states existed in the silica films and the stored carriers can serve as a “reservoir” for carrier transport. Based on the SCLC mechanism, the J - E relations can be quantitatively described as the following equation,

$$J = \varepsilon_r \times \varepsilon_0 \times \mu \times \frac{E^2}{d \times s},$$

where ε_0 is the permittivity of vacuum, and ε_r , μ , d , and s are the relative dielectric constant, carrier mobility of amorphous silica thin film, thickness of silica film, and injecting electrode area, respectively. By linearly fitting the $\log J$ - $\log E$ data as described in the black dot line of inset of figure 5e, the J - E relations present good linearity and carrier mobility μ can be calculated. The value of μ is mainly determined by the hopping processes. For pure silica film, the hopping processes only occur between trap states. The hopping-induced mobility can be evaluated by the following equation according to previous report (Please see Reference 30 in revised version),

$$u = \left(\frac{q}{k_0 T} \right) R^2 v_{ph} \times \exp \left(-\frac{2R}{a} - \frac{\Delta W}{K_0 T} \right),$$

where q is the charge of an electron, k_0 is the Boltzmann constant, T is the absolute temperature, R is the average separation in space, ΔW ($\sim k_0 T$) is the energy difference between the initial and final states involved in hopping, and a is the localization length, respectively. According to the reference [9], we use the values of a ($\sim 1nm$) and v_{ph} ($\sim 10^{12} s^{-1}$)s. As an estimation, we obtain the value of average separation in space is around 35 nm for trap defects existed in amorphous silica matrix.

In the absence of SnO₂ QD arrays in silica thin films, as shown in Figure 5a, EL can be measured only when the applied voltage is larger than $\sim 12V$. That is to say, the corresponding electric field is 1.2 MV/cm for the silica film with the thickness of 100 nm. The average acceleration length is 35 nm (the average separation of traps) and the corresponding electric field is 1.2MV/cm for pure silica film. Hence, the electrons can gain average energy exceeding 4 eV before being localized by the traps, which will give rise to elevate the electrons to the conduction bands of silica.

8. Flat-band energy level diagram of EL devices

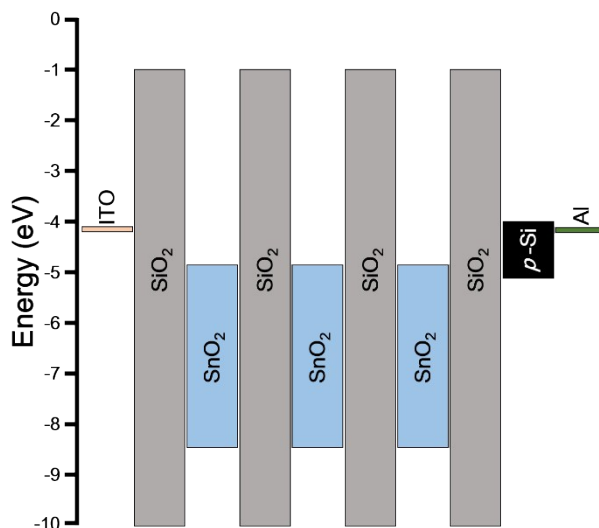


Figure S6. Flat-band energy level diagram of EL devices.

References

- [1] T. Lin, X. Zhang, Y. Wang, J. Xu, N. Wan, J. Liu, L. Xu, K. Chen, *Thin Solid Films* **2012**, 520, 5815.
- [2] T. Lin, X. Zhang, J. Xu, X. Liu, M. Swihart, L. Xu, K. Chen, *Appl. Phys. Lett.* **2013**, 103, 181906.
- [3] X. Zhang, T. Lin, P. Zhang, J. Xu, S. Lin, L. Xu, K. Chen, *Opt. Express* 2014, 22, 369.
- [4] X. Zhang, S. Lin, T. Lin, P. Zhang, J. Xu, L. Xu, K. Chen, *Phys. Chem. Chem. Phys.* **2015**, 17, 11974.
- [5] L. Brus, *J. Chem. Phys.* **1984**, 80, 4403.
- [6] J. T. Kong, H. M. Zhu, R. F. Li, W. Q. Luo, X. Y. Chen, *Opt. Lett.* **2009**, 34, 1873.
- [7] X. W. Zhang, T. Lin, P. Zhang, J. Xu, S. B. Lin, L. Xu, K. J. Chen, *Opt. Express* **2014**, 22, 369.
- [8] X. W. Zhang, T. Lin, J. Xu, L. Xu, K. J. Chen, *Chin. Phys. B* **2012**, 21(1), 018101.
- [9] K. Sun, W. Xu, B. Zhang, L. You, G. Ran, G. Qin, *Nanotechnology* **2008**, 19, 105708.

